Nanoscale

PAPER

View Article Online
View Journal | View Issue

Cite this: *Nanoscale*, 2016, **8**, 12977

Electrically conductive strain sensing polyurethane nanocomposites with synergistic carbon nanotubes and graphene bifillers†

Hu Liu,[a,b] Jiachen Gao,[a] Wenju Huang,[a] Kun Dai,*[a] Guoqiang Zheng,[a] Chuntai Liu,[a] Changyu Shen,[a] Xingru Yan,[b] Jiang Guo[b] and Zhanhu Guo*[b]

Received 16th March 2016,
Accepted 27th May 2016

DOI: 10.1039/c6nr02216b

www.rsc.org/nanoscale

Thermoplastic polyurethane (TPU) based conductive polymer composites (CPCs) with a reduced percolation threshold and tunable resistance–strain sensing behavior were obtained through the addition of synergistic carbon nanotubes (CNT) and graphene bifillers. The percolation threshold of graphene was about 0.006 vol% when the CNT content was fixed at 0.255 vol% that is below the percolation threshold of CNT/TPU nanocomposites. The synergistic effect between graphene and CNT was identified using the excluded volume theory. Graphene acted as a 'spacer' to separate the entangled CNTs from each other and the CNT bridged the broad gap between individual graphene sheets, which was beneficial for the dispersion of CNT and formation of effective conductive paths, leading to better electrical conductivity at a lower conductive filler content. Compared with the dual-peak response pattern of the CNT/TPU based strain sensors, the CPCs with hybrid conductive fillers displayed single-peak response patterns under small strain, indicating good tunability with the synergistic effect of CNT and graphene. Under larger strain, prestraining was adopted to regulate the conductive network, and better tunable single-peak response patterns were also obtained. The CPCs also showed good reversibility and reproductivity under cyclic extension. This study paves the way for the fabrication of CPC based strain sensors with good tunability.

1. Introduction

Polymer nanocomposites filled with functional nanofillers have been widely investigated in many fields, for example, strain sensors,[1–6] gas sensors,[7–11] giant magnetoresistance (GMR) sensors,[12–15] electromagnetic interference (EMI) shielding,[16–19] supercapacitors,[20] and environment remediation.[21,22] Among them, conductive polymer composite (CPC, normally consisting of insulating polymer and electrically conductive filler (carbon nanotube (CNT), carbon black (CB), graphene, carbon fiber (CF), intrinsically conductive polymers (PPy, PANI), nanometals, *etc.*[23–28])) based strain sensors, have shown great application potential due to their quick response to external stress on the basis of the merits of the polymer matrix properties including easy process and low manufacturing cost.[29,30] The strain response is usually addressed by noting the resistance variation upon applying an external strain, which was caused by the change of local contacts or tunneling distance between conductive fillers distributed in the polymer matrix. It is well known that the conductive network formed with conductive fillers provides the electrical conductivity of CPCs;[31] the morphology of the conductive network thus plays a crucial role in the strain sensing behaviors of CPCs upon applying an external strain. For example, Zhao *et al.* demonstrated that CPCs with a spherically shaped CB particle conductive network showed an increased response pattern during cyclic strain, and a decreased response pattern was obtained for the entangled CNT conductive network.[1] Liu *et al.* reported the strain sensing behavior of two-dimensional graphene filled thermoplastic polyurethane (TPU) conductive composites for the first time, and a two dimensional conductive network was achieved by the plane–plane contact of the flake-like graphene. High sensitivity and sensing stability were observed for different strain patterns together with good recoverability and reproducibility after stabilization by cyclic loading.[5] However, due to different demands for the strain sensing behavior in different applications, CPCs with tunable strain response patterns are needed.

[a]*School of Materials Science and Engineering, The Key Laboratory of Material Processing and Mold of Ministry of Education, Zhengzhou University, Zhengzhou, Henan 450001, China. E-mail: kundai@zzu.edu.cn*
[b]*Integrated Composites Laboratory (ICL), Department of Chemical & Biomolecular Engineering, University of Tennessee, Knoxville, TN 37996, USA. E-mail: zguo10@utk.edu*

†Electronic supplementary information (ESI) available. See DOI: 10.1039/c6nr02216b

Very recently, a combination of two or more kinds of conductive fillers in a polymer matrix has been demonstrated to be an effective method to construct a distinct conductive network morphology on the basis of the synergistic effect, which will endow CPCs with different sensing behaviors compared with the composites containing a single filler.[15,25,26,29] For example, Lin *et al.* added mixed CB and CNT into TPU to fabricate CPCs, and the influence of CB on the CPCs' strain sensitivity was investigated. The addition of CB is beneficial for the formation of fewer entangled CNT networks, which can be easily destructed under strain, showing a higher strain sensitivity.[25] Furthermore, the synergistic effect could also significantly reduce the percolation threshold (the concentration of a conductive filler at which an abrupt resistance variation occurred) of the CPCs, leading to good mechanical properties and lower cost.[32–37] For example, Zhao *et al.* prepared CB/CF/PP composites with segregated structures; CF acted as a bridge to come into contact with the segregated CB; thus effective conductive paths were formed and a lower percolation threshold was obtained.[37] Due to good electrical conductivity and a large aspect ratio, CNT based CPCs have been created, but the strong van der Waals force and the tangled structure of CNT make it difficult to be well dispersed in the polymer matrix, causing a higher percolation threshold.[38] Therefore, the addition of the secondary filler was adopted to improve its dispersion state and reduce the percolation threshold. For example, Socher *et al.* found that the addition of CB into CNT/polyamide 12 composites could effectively improve the CNT dispersion and reduce especially the size of big primary nanotube agglomerates, leading to a reduced percolation threshold.[39] Graphene, a single layer of carbon atoms with a two dimensional structure, has also been used to improve the dispersion of CNT due to its large specific surface area and intriguing low electrical resistivity. Hu *et al.* reported the preparation of graphene/CNT/silicone rubber composites; the physical isolation between graphene and CNT is formed with the addition of graphene, improving the dispersion of CNT and the conductivity of composites.[40] Nevertheless, the synergistic effect of graphene and CNT on the strain sensing properties has never been investigated.

TPU has been widely used in the fabrication of CPC based strain sensors due to its large elongation and good affinity with carbon fillers.[41–43] Herein, TPU based CPCs containing conducting CNT and a combination of hybrid CNT and graphene were fabricated. The electrical and thermal properties of the CPCs were studied. In order to confirm the existence of the synergy between graphene and CNT, field emission scanning electron microscopy (FE-SEM), transmission electron microscopy (TEM) and optical microscope images were recorded. The strain sensing behaviors of CNT/TPU and graphene/CNT/TPU were investigated respectively to study the synergistic effect on the strain sensing behavior. In addition, prestraining was adopted to regulate the strain sensing pattern. A sketch of the conductive network change under different strain conditions was also drawn to better understand the mechanism of the corresponding strain sensing pattern.

2. Experimental

2.1 Materials and CPC fabrication

Conducting fillers, amino CNT and graphene used in this study were supplied by Chengdu Organic Chemicals Co. Ltd, China. According to the supplier's specifications, the outer diameter and length of CNT were 8–15 and 50 nm, respectively. The $-NH_2$ content of CNT was about 0.45 wt%. The TEM image (Fig. 1(a)) shows CNTs entangled with each other. Graphene with a thickness ranging between 0.55 and 3.74 nm was dispersed in water and polyvinyl pyrrolidone was used as the dispersing agent. The wrinkled and crumpled structure of graphene was observed, Fig. 1(b). The hosting matrix was polyester-based thermoplastic polyurethane (TPU) (Elastollan 1185A, obtained from BASF Co. Ltd) with a density of 1.12 g cm^{-3} and a melt flow index of 17.5 g per 10 min (215 °C, at a pressure of 10 kg). Dimethylformamide (DMF) and methanol

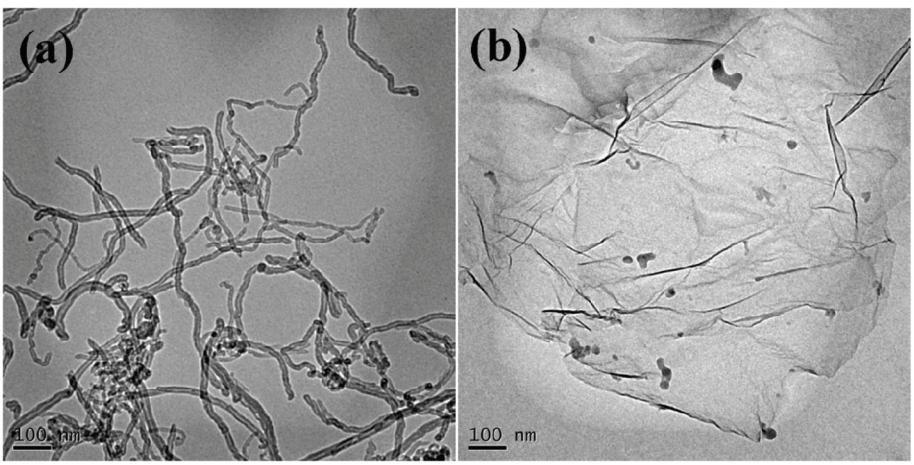

Fig. 1 Typical TEM images of (a) CNT and (b) graphene used in this study.

(Zhiyuan Reagent Co., Ltd, Tianjin, China) were used as received without any further treatment.

TPU based CPCs were fabricated using a co-coagulation plus compression molding method.[5] Briefly, the conducting fillers were first added into DMF and sonicated (285 W) for 10 min, and the mixture was then added to TPU/DMF solution (polymer loading was fixed at 5 wt%) and sonicated for 30 min. The blend was then added dropwise into methanol under vigorous stirring and black flocculate was obtained. The flocculate was then filtered, dried at 80 °C under vacuum for 20 h, and hot pressed at 210 °C for 10 min under a pressure of 15 MPa. The thickness of the sample was 0.5 mm. For CNT/TPU nanocomposites, different samples were prepared with 0.4–1.2 wt% CNT (the loading interval was 0.1 wt%). For hybrid graphene/CNT/TPU nanocomposites, the CNT content was fixed at 0.5 wt% (0.255 vol%), much lower than the percolation threshold of the CNT/TPU nanocomposites. The obtained hybrid nanocomposites were denoted $CNT_{0.5}/G_x$/TPU, where x = 0–0.12 wt% (the loading interval was 0.02 wt%). To convert the wt% loading of conductive fillers in the CPCs to vol%, the densities for graphene and CNT were both assumed to be 2.2 g cm^{-3} along with the known density of TPU, 1.12 g cm^{-3}.

2.2 Characterization

FE-SEM measurements were performed with a JEOL JSM-7500F instrument. The samples were prepared by immersing in liquid nitrogen for an hour and breaking quickly. The fracture surfaces were then coated with a thin layer of platinum for better imaging. TEM observation was performed with a JEOL JEM-1230 instrument at an acceleration voltage of 90 kV. The sample was prepared by embedding the CPCs in epoxy resin and cured at 70 °C for 24 h in a vacuum. Ultra-thin sections (~100 nm) were prepared using a Leica UC-7 ultramicrotome with a diamond knife at −90 °C. Optical microscope images were taken with an Olympus system BX51 in transmitted light configuration. Diluted conductive filler suspension was dropped on a glass slide to observe its dispersion state.

Differential scanning calorimetry (DSC) analysis were performed on a DISCOVERY DSC Q2920 instrument. The weight of each sample was about 8 mg. The samples were first heated to 220 °C at a heating rate of 10 °C min^{-1} and held isothermally for 5 min to erase the thermal history; then the samples were cooled down to −60 °C and reheated to 220 °C at the same rate. All the tests were performed under a nitrogen atmosphere at a flow rate of 20 mL min^{-1}.

X-ray diffraction (XRD) measurements were carried out using a Rigaku Ultima IV X-ray diffractometer, equipped with a Cu tube and a scintillation detector beam. The XRD scans were recorded from 5 to 80° for 2θ with a 0.02° step-width and a 60 s counting time for each step.

The rheological behaviors of pure TPU and its CPCs were studied with a rheometer (AR1500ex, TA Instruments). Environmental test chamber (ETC) steel parallel-plate geometry with a diameter of 25 mm was used to carry out the measurements. Dynamic oscillation frequency was swept from 100 to 0.1 Hz at a strain of 1% within the linear viscoelastic range at 200 °C under air atmosphere. The size of the samples for this test was 25 mm in diameter with around 2 mm thickness.

The volume resistance was measured using a precision digital resistor (Model TH2683, Changzhou Tonghui Electronics Co. Ltd, China) under a constant voltage of 10 V. Rectangular samples of 40 mm × 10 mm were cut from nanocomposite sheets with a thickness of 0.5 mm. The samples were clamped with a pair of aluminum electrodes and silver paste was used to ensure a good contact between the electrode and the sample. The volume conductivity was calculated by using the formula: $\sigma = L/RS$, where σ is the volume conductivity, R is the volume resistance, S is the cross-section area of the strip, and L is the length between the electrodes. For the strain sensing test, a gage length of 20 mm was created. The precision digital resistor and the universal testing machine were coupled with a computer to record the strain sensing behaviors upon cyclic loading online. The relative resistance was expressed by R/R_0, where R represents the transient resistance during the testing process, and R_0 is the initial resistance of the sample.

3. Results and discussion

3.1 Electrical properties of TPU based CPCs

Generally, the electrical conductivity (σ) of CPCs can be described in terms of modified classical percolation theory by using eqn (1):[45]

$$\sigma = \sigma_0(\phi - \phi_c)^t \quad (1)$$

where ϕ is the volume fraction of the fillers and ϕ_c is the percolation threshold, σ and σ_0 are the electrical conductivity of the CPCs at a given filler loading and the proportionality constant that is related to the intrinsic conductivity of the filler, respectively. The critical exponent t reflects the dimensionality of the conductive networks in the CPCs. The values of ϕ_c and t of CPCs were determined by fitting of the experimental data. The volume conductivities of the CPCs containing CNT or graphene alone as a function of filler content are plotted in Fig. 2(a). An ultralow percolation threshold of 0.051 vol% was estimated in the G/TPU nanocomposites due to the high electrical conductivity and good dispersion of graphene.[5] In addition, the CPCs containing CNT alone are observed to show a rapid increase in electrical conductivity by about 7 orders of magnitude (from 6.06×10^{-13} to 4.48×10^{-6} S cm^{-1}) when the CNT content was increased from 0.255 to 0.306 vol%, and a percolation threshold of about 0.337 vol% was estimated from the curve. The smaller percolation threshold of the CPCs containing graphene alone indicates that graphene possesses a better performance in improving the electrical conductivity of TPU than CNT. Although the inherently high conductivity and high aspect ratios of graphene and CNT allow them to form electrical pathways more easily in the polymer matrix, the morphology of the conductive filler also plays an important role in the geometry of the conductive network in the matrix.[44] The entangled structure of CNT (Fig. 1(a)) makes it difficult to be

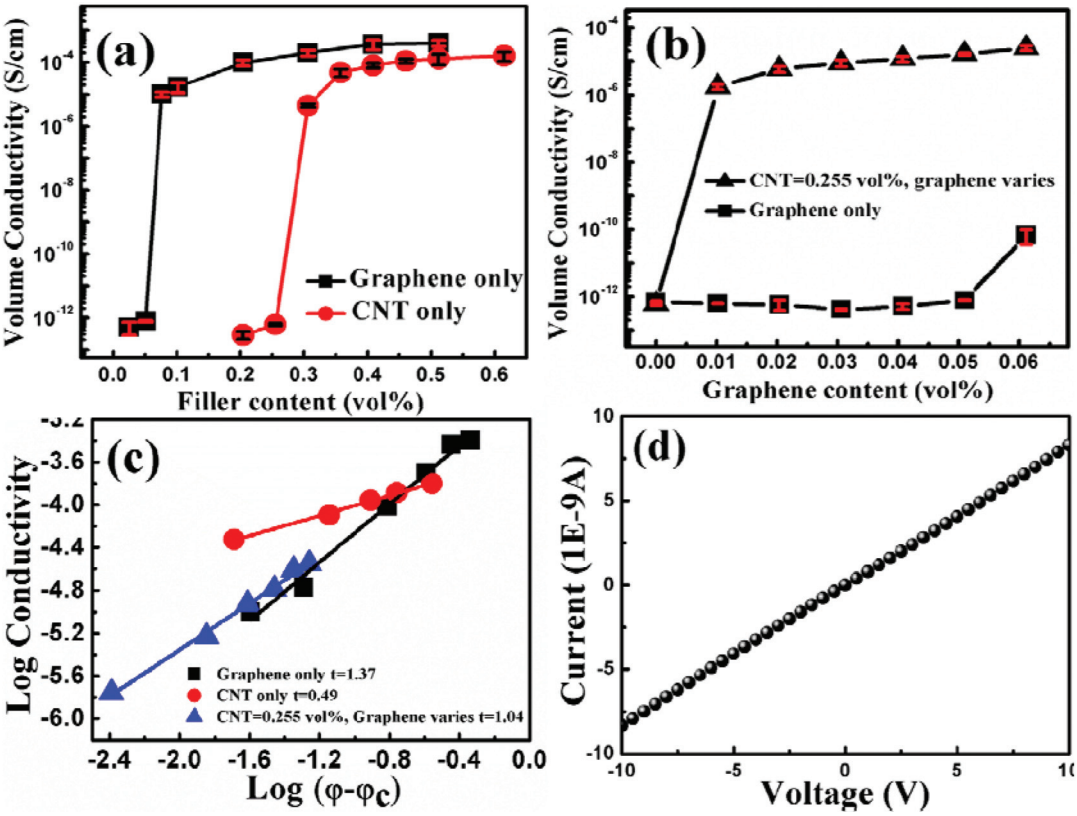

Fig. 2 Volume conductivity as a function of (a) CNT or graphene alone and (b) fixed CNT content of 0.255 vol% plus varying graphene content; (c) log conductivity *vs.* log($m - m_c$), where m is the filler mass content, m_c is the percolation threshold; (d) current–voltage (I–V) curves of the CPCs with hybrid fillers.

well dispersed in the TPU matrix, leading to a higher loading level for constructing effective conductive paths.

Furthermore, graphene was added in combination with CNT to investigate the synergistic effect on the electrical conductivity of TPU based CPCs. The CNT content was fixed at 0.255 vol% (lower than the percolation threshold of CNT/TPU nanocomposites) to explore the volume conductivity of the CPCs with hybrid fillers and the percolation threshold of graphene. As shown in Fig. 2(b), almost no enhancement in the conductivity was observed for the composites containing only 0 to 0.051 vol% graphene. However, a remarkable increase in electrical conductivity by about 7 orders of magnitude was observed for the hybrid nanocomposites when the graphene content was increased from 0 to 0.01 vol%, and the percolation threshold of graphene was calculated to be 0.006 vol%. Such superior electrical performances can certainly be attributed to the synergistic effect of the two-dimensional flexible graphene sheets and the one-dimensional CNT.

Finally, the critical resistance exponent t was used to explain the forming mechanism of the conductive network and the synergistic effect of the hybrid fillers (Fig. 2(c)). The values of t are estimated to be 1.37, 0.49 and 1.04 for CPCs with graphene only, CNT only and hybrid fillers (CNT + graphene), respectively. Generally, the t for a two-dimensional system is about 1.1–1.3 and between 1.6 and 2.0 for a three-dimensional system.[46] Thus, a nearly two-dimensional conductive network was constructed in G/TPU nanocomposites. For the CNT/TPU nanocomposites, the very low value indicates the disordered conductive network due to the entangled structure of CNT.[47] However, a nearly two-dimensional conductive network was formed with the addition of graphene (t = 1.04) for the hybrid composites, indicating that the coexistence of graphene and CNT was beneficial for the construction of ordered and perfect conductive paths. In addition, the current–voltage (I–V) characteristic of hybrid composites was studied, and a good linear ohmic behavior was observed (Fig. 2(d)), showing the stability of the conductive network composed of hybrid graphene and CNT, which was beneficial to obtain a stable electrical output signal when the CPCs were used as the strain sensor.

In order to estimate the synergistic effect of hybrid fillers, a model based on the excluded volume theory is applied and is expressed as eqn (2). The excluded volume is the volume around the object into which the center point of an identical object is prohibited.[48]

$$\frac{V_{\mathrm{CNT}}}{\phi_{\mathrm{CNT}}} + \frac{V_{\mathrm{graphene}}}{\phi_{\mathrm{graphene}}} = 1 \qquad (2)$$

where V_{CNT} and V_{graphene} are the volume content of CNT and graphene in the CNT/G/TPU composites, respectively, ϕ_{CNT}

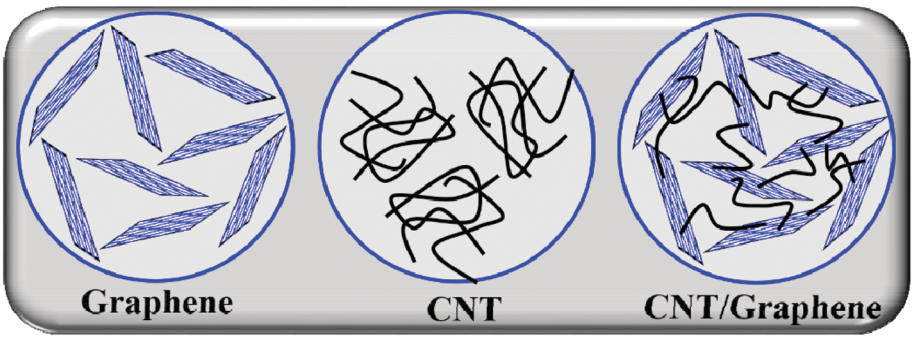

Fig. 3 Schematic illustrations of the synergistic effect between CNT and graphene.

and $\phi_{graphene}$ are the corresponding percolation thresholds when CNT or graphene is used alone. In general, the synergistic effect can be achieved only when the experimental percolation threshold is lower than the corresponding calculated volume content. In this case, V_{CNT}, ϕ_{CNT} and $\phi_{graphene}$ are 0.255, 0.337 and 0.051 vol%, respectively. Using eqn (2), the calculated volume content of graphene is 0.0124 vol%, higher than the experimental percolation threshold. It clearly indicates that the synergistic effect increased the conductivity of the CPCs with hybrid fillers.

To support the above observations, the synergistic effects are schematically illustrated in Fig. 3, where all fillers are well dispersed in the TPU matrix. In the TPU based nanocomposites containing graphene or CNT alone, the conductive paths are not constructed due to their low filler loadings, below the percolation thresholds of their nanocomposites. In addition, individual graphene sheets are homogeneously dispersed in the TPU matrix, but some CNTs are still intertwined with each other; herein a higher CNT loading is needed for the formation of effective conductive paths in the TPU matrix than that of graphene, causing a higher percolation threshold (Fig. 2(a)). However, once the graphene and CNT are added into the TPU matrix together, graphene acts as a 'spacer' to separate entangled CNTs from each other. Meanwhile, the CNT bridges the broad gap between individual graphene sheets, favoring the formation of more effective conductive paths.[49] Thus, the addition of a small amount of graphene could enhance the conductivity of CNT/TPU nanocomposites and reduce the percolation threshold of the nanocomposites effectively.

3.2 Dispersion characterization

3.2.1 Dispersion levels of conductive fillers. Optical microscope images were taken to observe the dispersion state of the conductive filler suspensions after the sonication treatment, Fig. 4. The images were taken 24 h after 30 min sonication. Due to the strong van der Waals force and the entangled structure of CNT, a homogeneous dispersion of CNT is hard to achieve, causing loosely stacked isolated aggregates of CNT (Fig. 4(a)). For the graphene/DMF suspension (Fig. 4(b)), the monolayer state of graphene was maintained after the sonication due to the existence of the dispersing agent polyvinyl pyrrolidone, and no aggregation was observed. However, the hybrid filler suspension shows a smaller cluster size and a more uniform distribution of CNT compared with the CNT/DMF suspension, Fig. 4(c). In addition, all the CNTs are observed to precipitate at the bottom of the bottle, Fig. 4(d), leaving a transparent supernatant. Meanwhile, the graphene solution retains its homogeneous state. However, almost no precipitation is found after the addition of graphene. All of these indicate that graphene has a dispersed effect in improving the CNT dispersion due to the large specific surface area and space hindrance effects of graphene. In addition, the overlaps between 1-dimensional CNT and 2-dimensional graphene benefit the formation of a more effective conductive network, resulting in a lower percolation threshold for hybrid systems.

3.2.2 Morphology of CPCs. In order to confirm the synergy between graphene and CNT, the dispersion state of hybrid conductive fillers in the TPU matrix was detected by FE-SEM and TEM. Fig. 5(a) displays the FE-SEM morphology of the freeze-fractured surface of the $CNT_{0.5}/G_{0.1}$/TPU composites. Homogeneously dispersed flake-like graphene is observed to be wrapped by the TPU matrix due to their good interfacial adhesion.[5] Taking a closer view (Fig. 5(b)), the CNTs (white dot) are seen uniformly embedded into TPU and adhered to graphene sheets. The good interfacial interaction between the N–H bond of CNT and the free C=O of TPU was also indicated in the FT-IR spectra of CNT/TPU composites (Fig. S1†). However, it cannot clearly reveal the morphology of the conductive network constructed by the synergistic effect of hybrid fillers. Hence, TEM was used to further identify it, and direct evidence for the synergy between graphene and CNT was strongly supported. The CNTs were uniformly dispersed and no aggregation was observed, Fig. 5(c). In addition, hair-like CNTs are observed to locate on the surface and act as a bridge to connect the separated graphene sheets, forming effective conductive paths; thus the addition of graphene benefits the dispersion of CNT and the reduction of the percolation threshold.

3.2.3 Rheological measurements. Generally, it is believed that the dispersion state of fillers in the polymer matrix can be evaluated by the rheological measurements.[5,50] The dependence of storage modulus (G') and loss modulus (G'') on the oscillatory frequency (Hz) of pure TPU and its CPCs at 200 °C is shown in Fig. 6. Over the range of oscillatory frequencies applied, pure TPU tended to exhibit a liquid-like terminal

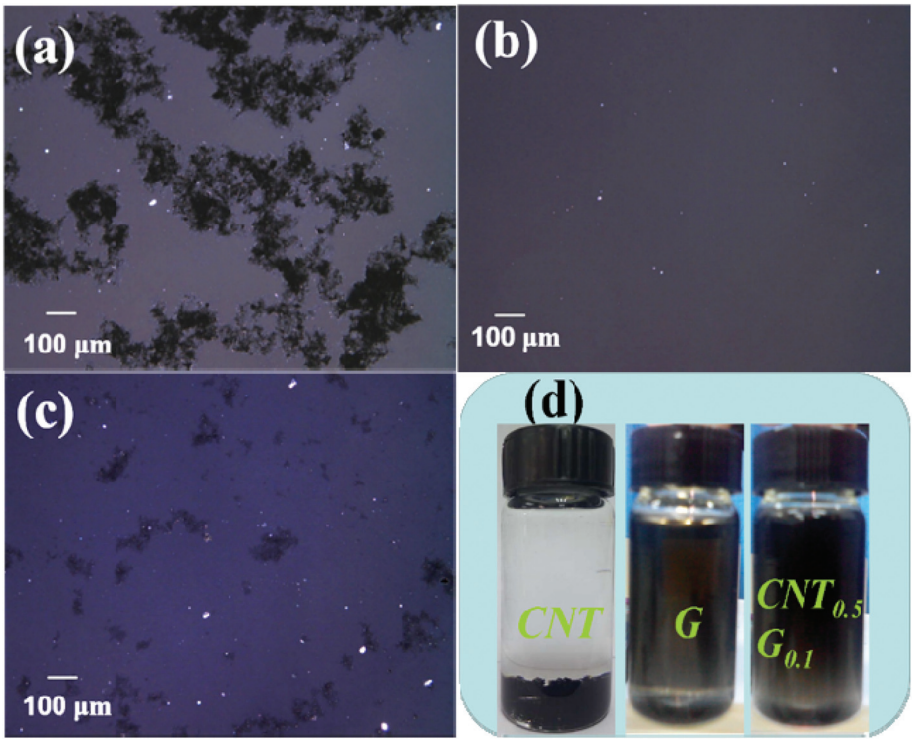

Fig. 4 Optical microscope images of suspensions: (a) CNT/DMF, (b) G/DMF, (c) $CNT_{0.5}/G_{0.1}$/DMF; (d) digital photos of conductive fillers/DMF suspensions, 24 h after sonication.

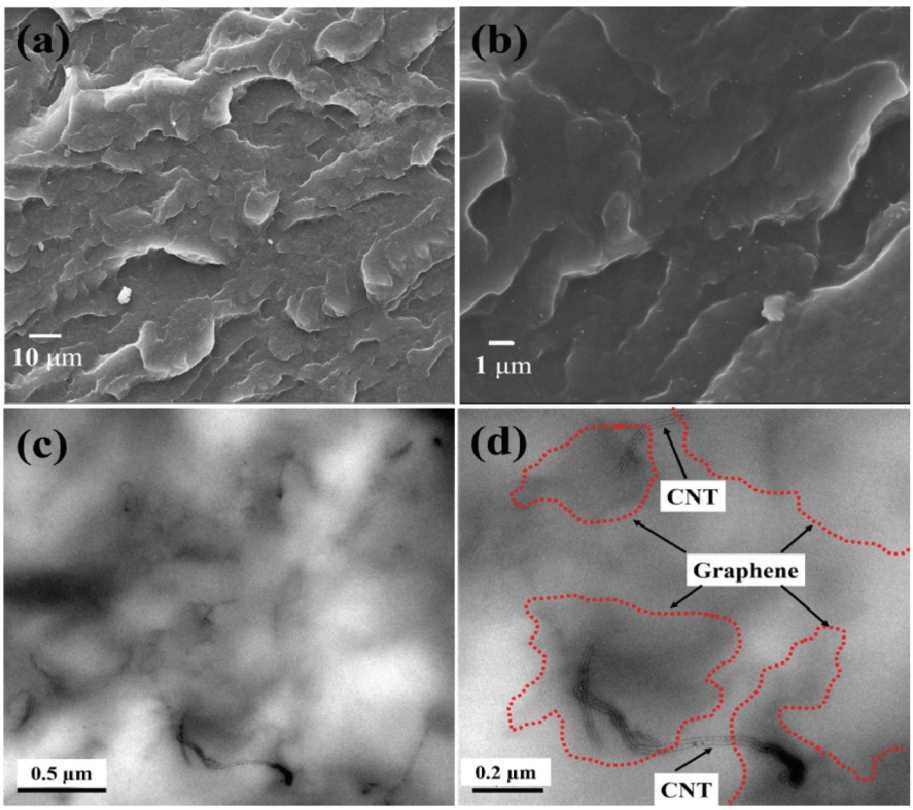

Fig. 5 (a & b) FE-SEM and (c & d) TEM images of CPCs containing 0.5 wt% CNT and 0.1 wt% graphene.

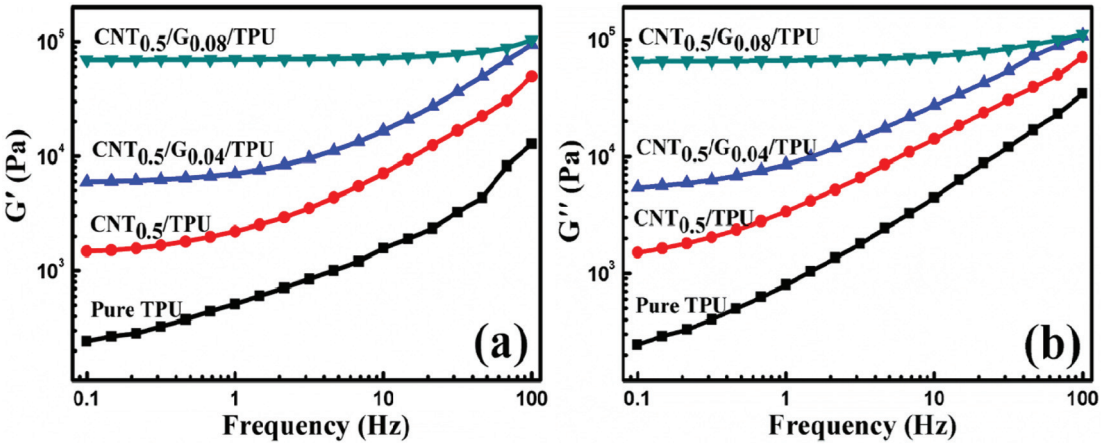

Fig. 6 Rheological behaviors of pure TPU and its CPCs containing different graphene loading levels by (a) storage modulus and (b) loss modulus *versus* frequency at 200 °C.

behavior.[51] For the CPCs containing 0.5 wt% CNT, the frequency dependent G' and G'' were influenced, especially at low frequencies. A modestly higher enhancement at low frequencies was obtained than that obtained at higher frequencies. However, remarkable increases for the whole angular frequency range and a plateau corresponding to a liquid-to-solid transition[51] were observed with the addition of only 0.08 wt% graphene, indicating the benefit of adding graphene for the formation of a pseudo solid-like network, possibly due to its greater interfacial contact area.[52] The results are attributed to the formation of effective conductive networks as a result of uniform dispersion of conductive fillers[53] due to the synergistic effect of graphene and CNT.

3.3 Thermal properties of composites

DSC experiments were carried out to investigate the effect of the incorporation of hybrid graphene and CNT on the thermal properties of TPU based CPCs, Fig. 7. The glass transition temperature (T_g) and melting temperature (T_m) are summarized in Table 1. Compared to pure TPU, a mild reduction of T_g and T_m was observed with the addition of 0.5 wt% CNT. However, both T_g and T_m were decreased obviously with increasing the graphene content. A reduction of about 4.27 and 6.62 °C was obtained for only 0.08 wt% graphene. This may be explained by the fact that the addition of graphene is beneficial for the dispersion of CNT in the TPU matrix, which will effectively block off the interconnected matrices to form confined regions of TPU chains in the composites. A higher loading of graphene means a more confined mobility of the polymer chains, which will lead to the formation of incomplete crystals with lower thermal stability during the crystallization. Thus, the T_m values of the composites showed a downward trend with increasing the graphene content.[54] In addition, a good dispersion of conductive fillers makes the entangled molecule chains in soft segments more loose, leading to easier mobility of soft segments and thus a reduced T_g.

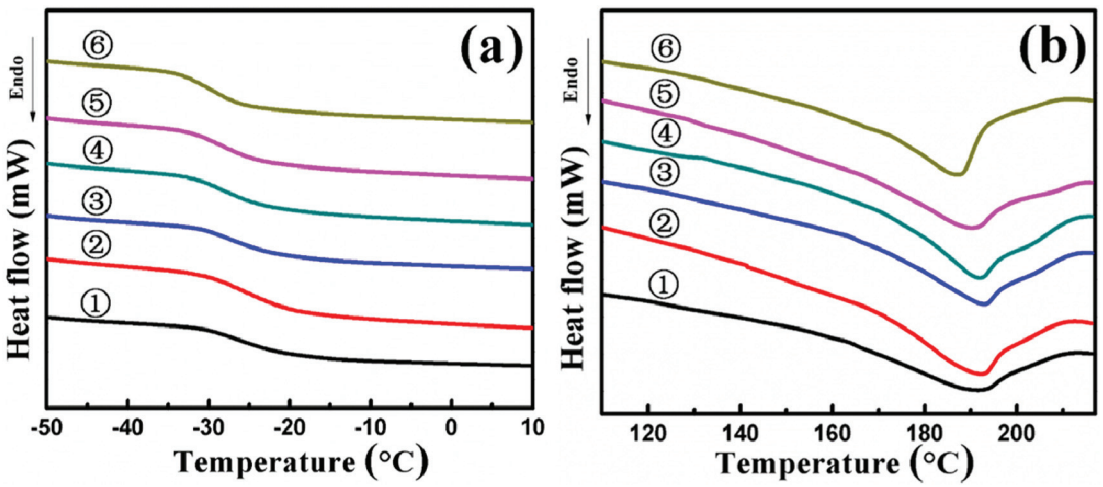

Fig. 7 (a) Glass transition curves and (b) melting curves of TPU and its CPCs. ① TPU; ② $CNT_{0.5}$/TPU; ③ $CNT_{0.5}/G_{0.02}$/TPU; ④ $CNT_{0.5}/G_{0.04}$/TPU; ⑤ $CNT_{0.5}/G_{0.06}$/TPU; ⑥ $CNT_{0.5}/G_{0.08}$/TPU.

Table 1 Thermal properties of TPU and its CPCs determined by DSC

Samples	TPU	$CNT_{0.5}$/TPU	$CNT_{0.5}/G_{0.02}$/TPU	$CNT_{0.5}/G_{0.04}$/TPU	$CNT_{0.5}/G_{0.06}$/TPU	$CNT_{0.5}/G_{0.08}$/TPU
T_g (°C)	−24.85	−25.14	−25.92	−26.89	−27.44	−29.12
T_m (°C)	192.52	192.26	192.42	191.8	189.16	186.9

3.4 XRD analysis

Fig. 8 displays the XRD profiles of graphene, CNT, TPU and $CNT_{0.5}/G_{0.08}$/TPU nanocomposites. Graphene is observed to exhibit a weak broad diffraction peak around 25.4°, which can be attributed to the (002) planes of a graphitic structure with short-range order in some stacked graphene sheets.[54,55] The disappearance of the diffraction peak in the G/TPU nanocomposites indicates that the graphene was well dispersed in the TPU matrix.[5] The diffraction peaks of CNT were observed at about 25.8° (002) and 43.3° (100), which were assigned to the interlayer space in the radial direction and the in-plane graphitic structure of CNT, respectively.[40] Moreover, pure TPU displays a diffraction peak at about 20.5°, which is relevant to the existence of a short range regular ordered structure of both hard and soft domains along with a disordered structure of the amorphous phase of the TPU matrix.[56] In the XRD profile of TPU/$CNT_{0.5}$/$graphene_{0.08}$ nanocomposites, except for the existence of the diffraction peak of TPU at 20.5°, the peak assigned to graphene disappeared, showing that good dispersion of graphene in TPU was not influenced by the presence of CNT. The almost complete disappearance of the peaks of CNTs at 25.8° and 43.3° may be due to the homogeneous dispersion of CNT in the TPU matrix.[57,58] All of these indicate that the addition of graphene favors the dispersion of CNT.

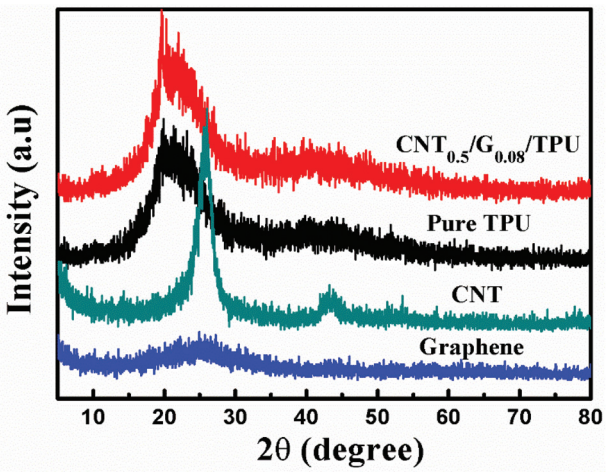

Fig. 8 XRD profiles of CNT, graphene, TPU, and $CNT_{0.5}/G_{0.08}$/TPU nanocomposites.

3.5 Strain sensing behavior of CPCs

The structure of the conductive network is known to govern the strain sensing behavior of CPCs. Thus, the cyclic extension was conducted on the CNT/TPU and CNT/G/TPU nanocomposites, respectively, and the synergistic effect of graphene on the strain response pattern of the CNT network was studied.[25] To acquire a stable output signal, the TPU nanocomposites containing 0.8 wt% CNT beyond the percolation threshold were first evaluated. First, the strain sensing behaviors of the TPU nanocomposites containing 0.8 wt% CNT subjected to a single cyclic extension with 5, 10 and 15% strain are shown in Fig. 9(a). For all the strain amplitudes, R/R_0 increases with increasing the strain during the extension process (this behavior can be defined as the positive strain effect), the increasing tendency originates from the destruction of partial conductive paths and the distance between CNTs (based on the model of the tunneling mechanism[59]), causing

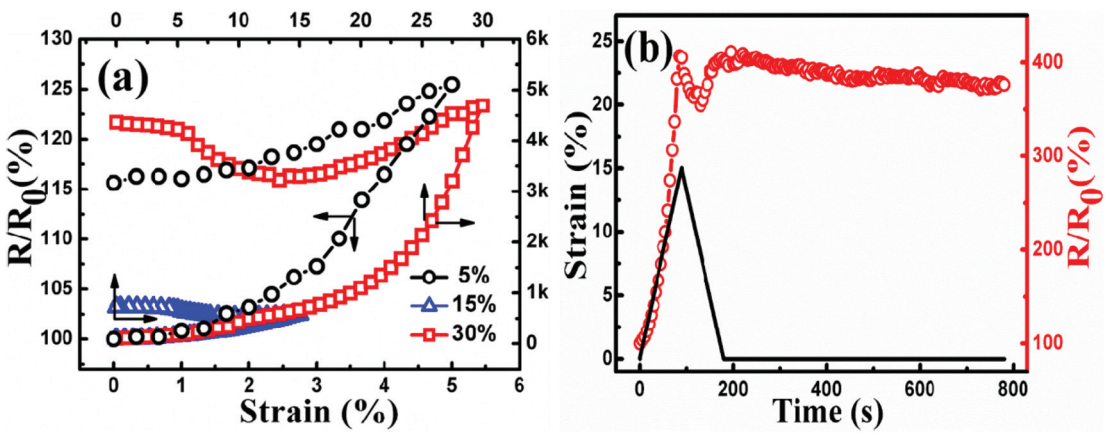

Fig. 9 (a) Resistance–strain behavior of TPU nanocomposites containing 0.8 wt% CNT up to 5 (the inset one), 15 and 30% strain at the strain rate of 0.1 min^{-1} in a single cycle; (b) R/R_0 variation of the CPCs when they were kept at 0% strain for 600 s after the unloading from 15% strain.

an increase of electrical resistance. Besides, the strain gauge factor (GF, which is defined as the relative resistance change divided by the applied strain[60]) was also used to evaluate the strain sensitivity of the CPCs. The GFs of the CPCs at a strain of 5, 15 and 30% were calculated to be 5.1, 32.09 and 152.93, respectively. It is evident that higher strain sensitivity was obtained at a larger strain; the distinct sensitivity was attributed to the large amount of breakdown in the conductive network under higher strain amplitude, causing larger variation in the electrical resistance. However, compared with the strain sensitivity of the G/TPU nanocomposites,[5] the CNT/TPU composites possess a higher one at the same strain amplitude, especially for the larger strains of 15 and 30%. This may be related to the microstructure of CNT and graphene (Fig. 1); the CNT conductive networks are easier to be disturbed by the external extension due to the point-to-point contacts between CNTs. However, it is believed that the plane-to-plane contacts between graphene construct more effective conductive paths, the contacts are not easy to be destroyed due to the large plane dimension of graphene.[61] The plate-like graphene possesses better surface attraction than the rod like CNT due to its larger specific surface area; thus the relative movement between graphene would be weaker than CNT when subjected to an external loading.[62] Hence, the CNT/TPU nanocomposites exhibit a larger increase of electrical resistance, and a higher strain sensitivity is obtained. During the releasing process, the reconstruction of conductive paths leads to a decline of the R/R_0, but a higher value than the initial one is obtained at the end of cyclic loading (usually called the residual resistance), showing that the conductive paths could not be fully recovered to their initial state. The hysteresis effect of the polymer macromolecular chains is usually used to explain this phenomenon.[63] As shown in Fig. 9(b), the CPCs were maintained at 0% strain for 600 s after the unloading from 15% strain, the R/R_0 was observed to still exhibit a downward trend and tended to be stable after the cyclic loading, which is a remarkable proof of the hysteresis effect resulting from the viscoelastic properties of the TPU.[64] But a large residual resistance is still observed after such a long recovery time; the permanent destruction of the conductive network due to the nonrecoverable change of TPU macromolecules plays an important role. In addition, a fluctuation appears during the releasing process arising from the competition between the destruction and reconstruction of the entangled CNT network.

Fig. 10(a) displays the strain sensing behavior during cyclic extension, a dual-peak pattern is observed (the inset). The 'main peak' corresponds to the sensitivity at the maximum strain in a single cycle; the 'shoulder peak' originates from the competition between the destruction and reconstruction of the conductive paths during the releasing process. For the application of a sensor, it is preferred to have a sharp 'main peak' and to eliminate the 'shoulder peak'. A similar behavior has been reported for the carbon black/elastomer nanocomposites.[65] However, the 'shoulder peak' for 15 and 30% strain is much more obvious than that for 5% strain. The small strain induces weak destruction of the entangled CNT network, so it is easy to recover after the release of external loading; however, the large strain seriously influences the entangled CNT network, the competition between the destruction and reconstruction of the conductive paths is remarkable during the contraction process. In addition, the R/R_0 upon extension first decreases with increasing the strain (this behavior can be defined as the negative strain effect) and then increases from the second cycle. There are two main aspects in this phenomenon. First, due to the existence of residual strain, the CPCs do not suffer from an external stress during the initial tension process, so the hysteresis effect makes the R/R_0 decrease continuously. Second, the competition between the destruction and reconstruction of the conductive paths plays a significant role.[66,67] Furthermore, the strain sensing behavior in each cycle shows a declining trend for a small strain (5%) with increasing the cycle number; however, the growing tendencies are observed for a large strain (15 and 30%). This is attributed to different destruction mechanisms of the conduc-

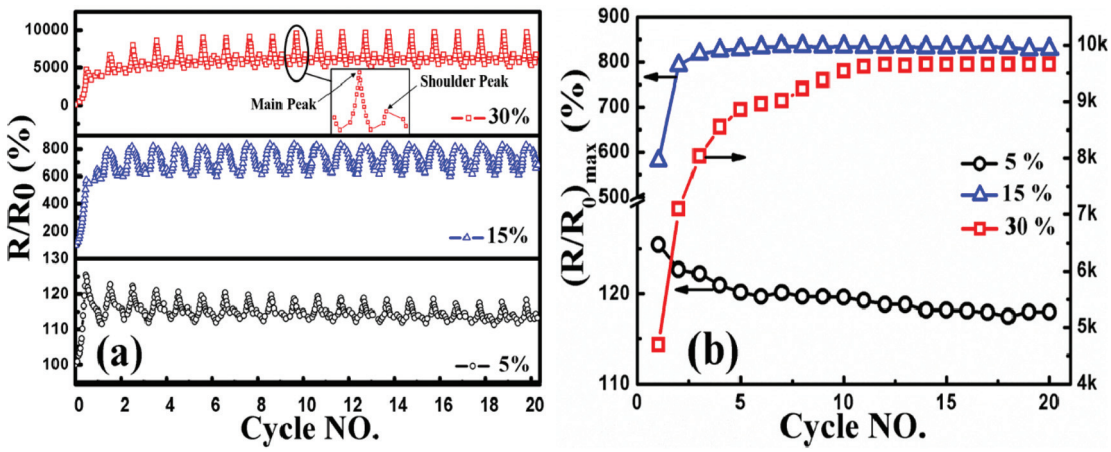

Fig. 10 (a) Resistance–strain behavior of TPU nanocomposites with 0.8 wt% CNT up to 5, 15 and 30% strain at the strain rate of 0.1 min^{-1} during cyclic extension; (b) the change of $(R/R_0)_{max}$ as a function of cycle number.

tive networks with different strain amplitudes. After the first extension cycle, although some permanent destruction of networks was caused due to the nonrecoverable polymer macromolecules, a more perfect CNT entangled structure was obtained for small strain amplitudes, leading to a smaller resistance variation for the following cycles. However, some entangled CNT can be stretched due to larger residual strain,[26] and can be separated from each other in the following extension process, showing a bigger resistance variation. Besides, the strain sensing behavior of the CPCs remains stable in each loop after several extension cycles, and the $(R/R_0)_{max}$ (R/R_0 value at the maximum strain in each cycle) reaches a constant value, Fig. 10(b), showing a good reversibility and reproductivity after the stabilization of cyclic loading. This indicates that the first several extension cycles have a stabilizing effect on the CNT conductive networks.

Due to the observed overlapping between CNT and graphene, the synergistic effect on the strain sensing behavior during the cyclic extension was studied. Fig. 11(a) shows the strain sensing behavior of the CNT/G/TPU nanocomposites with 0.5 wt% CNT and 0.1 wt% graphene in a single extension cycle with 5, 15 and 30% strain at a strain rate of 0.1 min^{-1}, a highest electrical conductivity was obtained at this filler ratio, which is beneficial to acquire a stable electrical output signal when subjected to external loading. Similar to the tendency of CPC containing single conducting fillers (CNT or graphene), a positive strain effect was observed during the extension process due to the destruction of conductive paths. During the releasing process, a residual resistance was obtained due to the existence of some permanent damaged conductive paths. In addition, the GFs of the CPCs at the strain of 5, 15 and 30% were calculated to be 3.58, 12.89 and 35.78, respectively. It is noted that the GF becomes smaller than the CPCs containing CNT only, especially under a larger strain, which is attributed to the synergistic effect of hybrid conducting fillers. For larger strain, the loosely entangled CNTs distributed in the CNT/TPU nanocomposites are stretched, and the CNTs are easier to be separated from each other, causing a serious resistance variation. However, for the conducting networks constituted by CNT and graphene, the synergistic effect benefits the formation of a stable conductive network, which is not easy to be destructed during the tension process; thus a lower sensitivity is obtained. Moreover, it can be seen that during the releasing process, a stable downward trend is observed and no fluctuation appears, showing that no competition between the destruction and construction of conductive paths occurs. A particular conductive network formed by the synergistic effect of CNT and graphene accounts for the distinct phenomenon. As discussed above, the fluctuation is mainly due to the entangled structure of CNT, which causes the competition between the destruction and reconstruction of conductive paths. However, the entangled CNTs were untied and their dispersion was also improved by the addition of graphene, and the overlaps between the CNT and graphene formed the main conductive paths (Fig. 5(d)). Thus, the conductive paths would break up and come into contact with each other directly, without the occurrence of competition. Fig. 11(b) depicts the strain sensing behaviors of CPCs containing hybrid conducting fillers under 20 cyclic extensions. Compared with the strain sensing behavior of CNT/TPU strain sensors, the 'shoulder peak' disappears and a single-peak response pattern with good reproductivity is obtained for 5% strain amplitude as the cycle number increases, showing a good tunability with the synergistic effect of the hybrid conductive fillers. However, the strain sensing behavior shows an increasing trend and a dual-peak response pattern appears again for 15 and 30% strain amplitude. Different response patterns indicate that the hybrid conducting network possesses good stability under lower strain amplitude, but it is easy to be destroyed when subjected to larger strain amplitude.

To better understand the mechanism of CPCs under different strains, a schematic representation of the change of the graphene and CNT conductive network is proposed in Fig. 12. In the initial state, perfect conductive paths were formed by the connected graphene and CNT. When the CPCs are stretched to a small strain (5%), the distance between con-

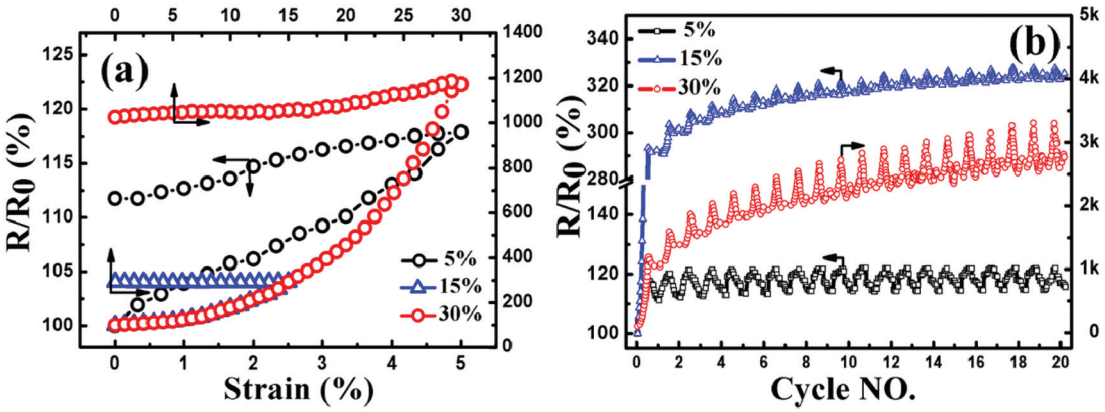

Fig. 11 Resistance–strain behavior of the TPU nanocomposites with 0.5 wt% CNT and 0.1 wt% graphene, up to 5, 15 and 30% strain at the strain rate of 0.1 min^{-1} (a) in a single extension cycle and (b) during cyclic extension.

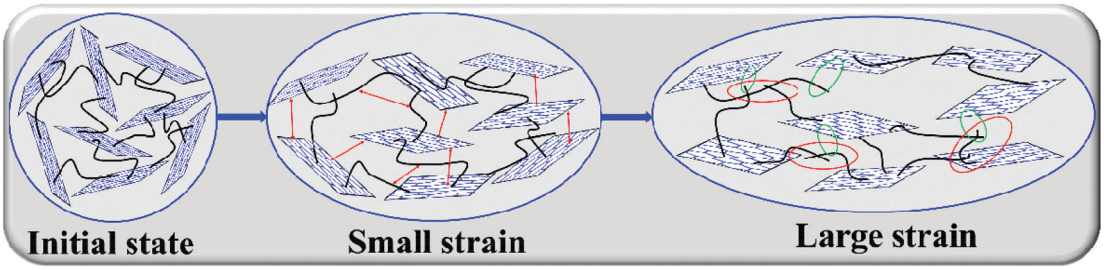

Fig. 12 Sketch of the change of graphene and CNT conductive networks under different strains.

ductive fillers increases (red line), causing a higher resistance. Based on the tunneling junction gap width modulation described by the fluctuation-induced tunneling (FIT) model,[68] the increased tunneling distance induced by the external strain accounts for the increased resistance under a small strain.[26,62,69] But the morphology of the conductive network almost remains unchanged; thus the strain sensing behavior possesses good reversibility and reproductivity. For a larger strain (15 and 30%), some conductive paths were broken down (green ellipse) and thus had a serious influence on the electrical resistance of CPCs, so a higher sensitivity was obtained. In addition, some CNTs are intertwined with each other again (red ellipse), causing the formation of a disordered network structure. Hence, the same mechanism as for the CNT/TPU nanocomposites, a competition between the destruction and reconstruction, appears again upon the cyclic loading.

Generally, the single-peak response pattern is better for establishing the relationship between resistance and strain than the dual-peak one. Besides, it is also beneficial for practical applications of strain sensors. The dependence of electrical resistance on strain could be modified through pre-straining.[62] Fig. 13(a) displays the strain sensing behavior of the CPCs for the strain between 5 and 20%; a single-peak response pattern was observed. The change of sensing behavior under the same strain amplitude is mainly relevant to the extension style. As discussed above, the conductive network is in a disordered state when the CPCs are released to the 0 strain; the competition between destruction and reconstruction of conductive paths induces the appearance of a dual-peak response pattern. However, the conductive network is still in an ordered tension state when the composites are released to 5% strain; thus a single-peak response pattern is observed with the cyclic extension. In addition, the strain sensing behavior increases gradually with increasing the cycle number due to the additional breakdown of the conductive network; but it tends to be constant with the stabilization of the conductive network under cyclic extension.

After 20 cycles of prestraining for about 24 h, the same samples were tested again for cyclic extension for strain between 0 and 15%, Fig. 13(b). Interestingly, the samples exhibit a positive strain effect and a single-peak response pattern with a good reversibility and reproductivity is observed. This indicates that prestraining between 5 and 20% is beneficial for the formation of ordered and stable conductive networks. Further, a reduction of strain sensitivity was observed after the prestraining. It may be explained by the fact that imperfect conductive paths have been destroyed during the prestraining cycles; thus the variation of resistance during the extension process becomes smaller, showing lower strain sensitivity. In addition, the $CNT_{0.5}/G_{0.1}$/TPU composites possess an elongation at break of about 90% (Fig. S2†) due to the good elasticity of TPU, indicating that the CPCs have a great potential in the application of detecting a larger strain.

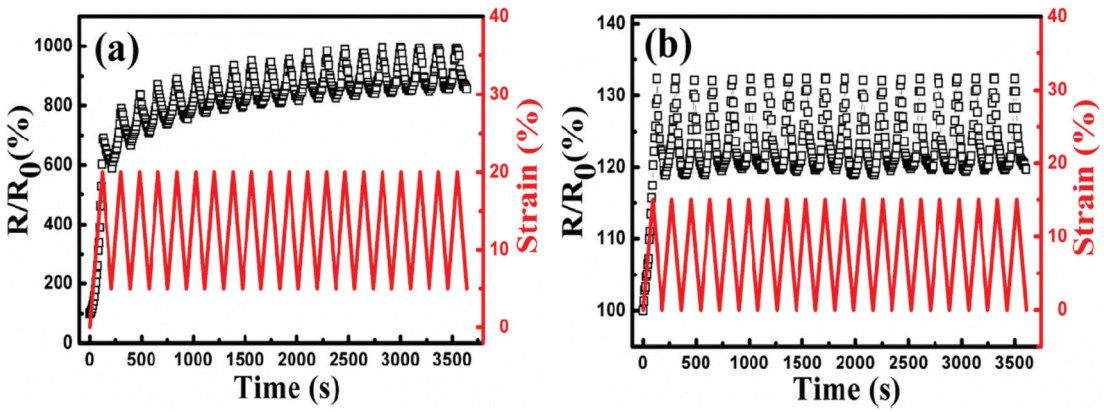

Fig. 13 Strain sensing behaviors of nanocomposites for (a) strains between 5 and 20%, and (b) strains between 0 and 15% after the prestraining for about 24 h.

4. Conclusions

Electrically conductive CNT/G/TPU nanocomposites were fabricated and their feasibility to serve as the strain sensors was justified. Compared with the CNT/TPU nanocomposites, a remarkable increase in the electrical conductivity by about 7 orders of magnitude was observed for the hybrid nanocomposites when the graphene content was increased from 0 to 0.01 vol%, and a very small percolation threshold of 0.006 vol% was obtained. The synergistic effect between graphene and CNT was identified using the excluded volume theory. The improved dispersion of CNT with the assistance of graphene was observed from the optical microscope images. In addition, graphene acted as a 'spacer' to separate entangled CNTs from each other and the CNT bridged the broad gap between individual graphene sheets as seen from the FE-SEM and TEM images. The results of XRD and rheology also proved the uniform dispersion of the hybrid conductive fillers. All these benefited from the synergistic effect between graphene and CNT, which facilitated the formation of effective conductive paths, leading to a better electrical conductivity. Compared with CNT/TPU nanocomposites, the good dispersion of the hybrid conductive filler endowed the hybrid CPCs containing only 0.08 wt% graphene with a reduction of about 4.27 and 6.62 °C for T_g and T_m, respectively. As a strain sensor, lower strain sensitivity was observed for the hybrid CPCs than that for the CPCs containing CNT only, especially under a larger strain. The conducting networks constituted by CNT and graphene were not easier to be broken down than the conducting networks containing CNT alone. During 20 cyclic extensions, it showed a perfect single-peak response pattern with good reversibility and reproductivity under small strain, showing a good tunability with the synergistic effect of the hybrid conductive fillers. But the dual-peak response pattern appeared gradually again after several cycles for larger strain. This indicates that the hybrid conducting networks possessed good stability under lower strain amplitude, but their stability was easy to be destroyed when subjected to larger strain amplitude. Prestraining was adopted to regulate the conductive network under larger strain amplitude, and a good single-peak response pattern with good reversibility and reproductivity was also acquired. This study paves the way for the fabrication of CPC based strain sensors with good tunability.

Acknowledgements

The authors gratefully acknowledge the financial support of this work by the National Natural Science Foundation (contract number 11572290 and 11432003), China Postdoctoral Science Foundation (contract number 2015M580637), and Special Science Foundation for Excellent Youth Scholars of Zhengzhou University (contract number 1421320041). Z. Guo appreciates the start-up fund from University of Tennessee Knoxville. H. Liu acknowledges the support from the China Scholarship Council.

References

1 J. Zhao, K. Dai, C. Liu, G. Zheng, B. Wang, C. Liu, J. Chen and C. Shen, *Composites, Part A*, 2013, **48**, 129–136.
2 L. Lin, S. Liu, S. Fu, S. Zhang, H. Deng and Q. Fu, *Small*, 2013, **9**, 3620–3629.
3 V. Eswaraiah, K. Balasubramaniam and S. Ramaprabhu, *J. Mater. Chem.*, 2011, **21**, 12626–12628.
4 (*a*) D. Ding, H. Wei, J. Zhu, Q. He, X. Yan, S. Wei and Z. Guo, *Energy Environ. Focus*, 2014, **3**, 85–93; (*b*) Q. He, T. Yuan, X. Zhang, S. Guo, J. Liu, J. Liu, X. Liu, L. Sun, S. Wei and Z. Guo, *Mater. Res. Express*, 2014, **1**, 035029.
5 H. Liu, Y. Li, K. Dai, G. Zheng, C. Liu, C. Shen, X. Yan, J. Guo and Z. Guo, *J. Mater. Chem. C*, 2016, **4**, 157–166.
6 H. Liu, W. Huang, J. Gao, K. Dai, G. Zheng, C. Liu, C. Shen, X. Yan, J. Guo and Z. Guo, *Appl. Phys. Lett.*, 2016, **1**, 011904.
7 Y. Li, H. Liu, K. Dai, G. Zheng, C. Liu, J. Chen and C. Shen, *Sens. Actuators, B*, 2015, **221**, 1279–1289.
8 K. Li, K. Dai, X. Xu, G. Zheng, C. Liu, J. Chen and C. Shen, *Colloid Polym. Sci.*, 2013, **291**, 2871–2878.
9 W. Yuan, L. Huang, Q. Zhou and G. Shi, *ACS Appl. Mater. Interfaces*, 2014, **6**, 17003–17008.
10 Q. Fan, Z. Qin, T. Villmow, J. Pionteck, P. Pötschke, Y. Wu, B. Voit and M. Zhu, *Sens. Actuators, B*, 2011, **156**, 63–70.
11 H. Bai, K. Sheng, P. Zhang, C. Li and G. Shi, *J. Mater. Chem.*, 2011, **21**, 18653–18658.
12 H. Gu, Y. Huang, X. Zhang, Q. Wang, J. Zhu, L. Shao, N. Haldolaarachchige, D. P. Young, S. Wei and Z. Guo, *Polymer*, 2012, **53**, 801–809.
13 B. Qiu, J. Guo, Y. Wang, X. Wei, Q. Wang, D. Sun, M. A. Khan, D. P. Young, R. O'Connor, X. Huang, X. Zhang, B. L. Weeks, S. Wei and Z. Guo, *J. Mater. Chem. C*, 2015, **3**, 3989–3998.
14 Z. Guo, H. T. Hahn, H. Lin, A. B. Karki and D. P. Young, *J. Appl. Phys.*, 2008, **104**, 014314.
15 H. Gu, J. Guo, H. Wei, S. Guo, J. Liu, Y. Huang, M. A. Khan, X. Wang, D. P. Young, S. Wei and Z. Guo, *Adv. Mater.*, 2015, **27**, 6277–6282.
16 S. P. Pawar, D. A. Marathe, K. Pattabhi and S. Bose, *J. Mater. Chem. A*, 2015, **3**, 656–669.
17 Q. He, T. Yuan, X. Zhang, X. Yan, J. Guo, D. Ding, M. A. Khan, D. P. Young, A. Khasanov, Z. Luo, J. Liu, T. D. Shen, X. Liu, S. Wei and Z. Guo, *J. Phys. Chem. C*, 2014, **118**, 24784–24796.
18 J. Zhu, S. Wei, N. Haldolaarachchige, D. P. Young and Z. Guo, *J. Phys. Chem. C*, 2011, **115**, 15304–15310.
19 D. X. Yan, H. Pang, L. Xu, Y. Bao, P. G. Ren, J. Lei and Z. M. Li, *Nanotechnology*, 2014, **25**, 145705.
20 D. Li, Y. Liu, B. Lin, C. Lai, Y. Sun, H. Yang and X. Zhang, *RSC Adv.*, 2015, **5**, 98278–98287.
21 D. Zhang, S. Wei, C. Kaila, X. Su, J. Wu, A. B. Karki, D. P. Young and Z. Guo, *Nanoscale*, 2010, **2**, 917–919.
22 J. Zhu, S. Wei, M. Chen, H. Gu, S. B. Rapole, S. Pallavkar, T. C. Ho, J. Hopper and Z. Guo, *Adv. Powder Technol.*, 2013, **24**, 459–467.
23 C. Yan, J. Wang, W. Kang, M. Cui, X. Wang, C. Y. Foo, K. J. Chee and P. S. Lee, *Adv. Mater.*, 2014, **26**, 2022–2027.

24 M. Z. Seyedin, J. M. Razal, P. C. Innis and G. G. Wallace, *Adv. Funct. Mater.*, 2014, **24**, 2957–2966.
25 L. Lin, S. Liu, Q. Zhang, X. Li, M. Ji, H. Deng and Q. Fu, *ACS Appl. Mater. Interfaces*, 2013, **5**, 5815–5824.
26 L. Lin, H. Deng, X. Gao, S. Zhang, E. Bilotti, T. Peijs and Q. Fu, *Polym. Int.*, 2013, **62**, 134–140.
27 M. Li, H. Li, W. Zhong, Q. Zhao and D. Wang, *ACS Appl. Mater. Interfaces*, 2014, **6**, 131–1319.
28 (*a*) H. Liu, W. Huang, X. Yang, K. Dai, G. Zheng, C. Liu, C. Shen, X. Yan, J. Guo and Z. Guo, *J. Mater. Chem. C*, 2016, **4**, 4459–4469; (*b*) Y. Lan, H. Liu, X. Cao, S. Zhao, K. Dai, X. Yan, G. Zheng, C. Liu, C. Shen and Z. Guo, *Polymer*, 2016, **97**, 11–19.
29 (*a*) D. Ponnamma, K. K. Sadasivuni, M. Strankowski, Q. Guo and S. Thomas, *Soft Matter*, 2013, **9**, 10343–10353; (*b*) J. Gu, X. Yang, Z. Lv, N. Li, C. Liang and Q. Zhang, *Int. J. Heat Mass Transfer*, 2016, **92**, 15–22.
30 (*a*) H. Wei, D. Ding, S. Wei and Z. Guo, *J. Mater. Chem. A*, 2013, **1**, 10805–10813; (*b*) J. Gu, N. Li, L. Tian, Z. Lv and Q. Zhang, *RSC Adv.*, 2015, **5**, 36334–36339.
31 C. Mao, Y. Zhu and W. Jiang, *ACS Appl. Mater. Interfaces*, 2012, **4**, 5281–5286.
32 A. S. Patole, S. P. Patole, S.-Y. Jung, J.-B. Yoo, J.-H. An and T.-H. Kim, *Eur. Polym. J.*, 2012, **48**, 252–259.
33 H. Palza, B. Reznik, M. Wilhelm, O. Arias and A. Vargas, *Macromol. Mater. Eng.*, 2012, **297**, 474–480.
34 A. K. Keshri, J. Huang, V. Singh, W. Choi, S. Seal and A. Agarwal, *Carbon*, 2010, **48**, 431–442.
35 E. Bilotti, H. Zhang, H. Deng, R. Zhang, Q. Fu and T. Peijs, *Compos. Sci. Technol.*, 2013, **74**, 85–90.
36 S. Zhang, S. Yin, C. Rong, P. Huo, Z. Jiang and G. Wang, *Eur. Polym. J.*, 2013, **49**, 3125–3134.
37 S. Zhao, H. Zhao, G. Li, K. Dai, G. Zheng, C. Liu and C. Shen, *Mater. Lett.*, 2014, **129**, 72–75.
38 T. Fukushima, A. Kosaka, Y. Yamamoto, T. Aimiya, S. Notazawa, T. Takigawa, T. Inabe and T. Aida, *Small*, 2006, **2**, 554–560.
39 R. Socher, B. Krause, S. Hermasch, R. Wursche and P. Pötschke, *Compos. Sci. Technol.*, 2011, **71**, 1053–1059.
40 H. Hu, L. Zhao, J. Liu, Y. Liu, J. Cheng, J. Luo, Y. Liang, Y. Tao, X. Wang and J. Zhao, *Polymer*, 2012, **53**, 3378–3385.
41 Q. Fan, Z. Qin, S. Gao, Y. Wu, J. Pionteck, E. Mäder and M. Zhu, *Carbon*, 2012, **50**, 4085–4092.
42 M. Ji, H. Deng, D. Yan, X. Li, L. Duan and Q. Fu, *Compos. Sci. Technol.*, 2014, **92**, 16–26.
43 S. Shang, W. Zeng and X.-m. Tao, *J. Mater. Chem.*, 2011, **21**, 7274.
44 T. W. Yoo, Y. K. Lee, S. J. Lim, H. G. Yoon and W. N. Kim, *J. Mater. Sci.*, 2013, **49**, 1701–1708.
45 J.-C. Huang, *Adv. Polym. Technol.*, 2002, **21**, 299–313.
46 S. J. Babinec, R. D. Mussell, R. L. Lundgard and R. Cieslinski, *Adv. Mater.*, 2000, **12**, 1823–1834.
47 K. Dai, X.-B. Xu and Z.-M. Li, *Polymer*, 2007, **48**, 849–859.
48 H.-D. B. Yao Sun, Z.-X. Guo and J. Yu, *Macromolecules*, 2009, **42**, 459–463.
49 T. Wei, L. Song, C. Zheng, K. Wang, J. Yan, B. Shao and Z.-J. Fan, *Mater. Lett.*, 2010, **64**, 2376–2379.
50 L. Yue, G. Pircheraghi, S. A. Monemian and I. Manas-Zloczower, *Carbon*, 2014, **78**, 268–278.
51 T. Chatterjee and R. Krishnamoorti, *Soft Matter*, 2013, **9**, 9515.
52 X. Y. Qi, D. Yan, Z. Jiang, Y. K. Cao, Z. Z. Yu, F. Yavari and N. Koratkar, *ACS Appl. Mater. Interfaces*, 2011, **3**, 3130–3133.
53 E. E. Ureña-Benavides, M. J. Kayatin and V. A. Davis, *Macromolecules*, 2013, **46**, 1642–1650.
54 J. Zhao, X. Wang, W. Zhou, E. Zhi, W. Zhang and J. Ji, *J. Appl. Polym. Sci.*, 2013, **130**, 3212–3220.
55 G. Wang, Z. Gao, G. Wan, S. Lin, P. Yang and Y. Qin, *Nano Res.*, 2014, **7**, 704–716.
56 H.-C. Kuan, C.-C. M. Ma, W.-P. Chang, S.-M. Yuen, H.-H. Wu and T.-M. Lee, *Compos. Sci. Technol.*, 2005, **65**, 1703–1710.
57 T. McNally, P. Pötschke, P. Halley, M. Murphy, D. Martin, S. E. J. Bell, G. P. Brennan, D. Bein, P. Lemoine and J. P. Quinn, *Polymer*, 2005, **46**, 8222–8232.
58 S. Shang, L. Gan, M. C.-w. Yuen, S.-x. Jiang and N. Mei Luo, *Composites, Part A*, 2014, **66**, 135–141.
59 I. Balberg, *Phys. Rev. Lett.*, 1987, **59**, 1305–1308.
60 P. Slobodian, P. Riha and P. Saha, *Carbon*, 2012, **50**, 3446–3453.
61 J. Du, L. Zhao, Y. Zeng, L. Zhang, F. Li, P. Liu and C. Liu, *Carbon*, 2011, **49**, 1094–1100.
62 H. Yazdani, K. Hatami, E. Khosravi, K. Harper and B. P. Grady, *Carbon*, 2014, **79**, 393–405.
63 J.-H. Kong, N.-S. Jang, S.-H. Kim and J.-M. Kim, *Carbon*, 2014, **77**, 199–207.
64 L. Supriya, S. Unal, T. E. Long and R. O. Claus, *Chem. Mater.*, 2006, **18**, 2506–2512.
65 K. Yamaguchi, J. J. C. Busfield and A. G. Thomas, *J. Polym. Sci., Part B: Polym. Phys.*, 2003, **41**, 2079–2089.
66 R. Zhang, H. Deng, R. Valenca, J. Jin, Q. Fu, E. Bilotti and T. Peijs, *Sens. Actuators, A*, 2012, **179**, 83–91.
67 R. Zhang, H. Deng, R. Valenca, J. Jin, Q. Fu, E. Bilotti and T. Peijs, *Compos. Sci. Technol.*, 2013, **74**, 1–5.
68 R. Zhang, M. Baxendale and T. Peijs, *Phys. Rev. B: Condens. Matter*, 2007, **76**, 195433.
69 E. Bilotti, R. Zhang, H. Deng, M. Baxendale and T. Peijs, *J. Mater. Chem.*, 2010, **20**, 9449–9455.